# Comparative study of the surface layer density of liquid surfaces

E. Chacón,[1,2,*] E. M. Fernández,[1] D. Duque,[3,†] R. Delgado-Buscalioni,[3] and P. Tarazona[3,2]

[1]*Instituto de Ciencia de Materiales de Madrid, CSIC, E-28049 Madrid, Spain*
[2]*Instituto Nicolás Cabrera, Universidad Autónoma de Madrid, E-28049 Madrid, Spain*
[3]*Departamento de Física Teórica de la Materia Condensada (C-V), Universidad Autónoma de Madrid, E-28049 Madrid, Spain*

Capillary wave fluctuations blur the inherent structure of liquid surfaces in computer simulations. The intrinsic sampling method subtracts capillary wave fluctuations and yields the intrinsic surface structure, leading to a generic picture of the liquid surface. The most relevant magnitude of the method is the surface layer density $n_s$ that may be consistently determined from different properties: the layering structure of the intrinsic density profiles, the turnover rate for surface layer particles, and the hydrodynamic damping rate of capillary waves. The good agreement among these procedures provides evidence for the physical consistency of the surface layering hypothesis, as an inherent physical property of the liquid surfaces. The dependence of the surface compactness, roughness, and exchange rate with temperature is analyzed for several molecular interaction models.

## I. INTRODUCTION

Computer simulations and experimental studies of fluid interfaces face the blurring effects of thermal capillary waves (CWs) that increase with the sampled transverse area $A_0$, and precludes a sharp molecular view of the interfacial structure. In the usual description, the mean density profile $\rho(z, A_0)$ becomes a smoother function of the normal coordinate $z$, as $A_0$ grows. Capillary wave theory[1–3] (CWT) provides the framework to analyze surface fluctuations, and the induced dependence on $A_0$. The theory postulates that each molecular configuration of a liquid surface has an intrinsic surface $z = \xi(\mathbf{R}, q_u)$, with $\mathbf{R} = (x, y)$, to represent the instantaneous molecular frontier between the liquid and vapor phases. We keep explicit the dependence of the intrinsic surface on the *upper* wave vector cutoff $q_u$. The statistical average of the molecular density referred to the intrinsic surface is the *intrinsic* density profile,

$$\tilde{\rho}(z, q_u) = \left\langle \frac{1}{A_0} \sum_{i=1}^{N} \delta(z - z_i + \xi(\mathbf{R}_i, q_u)) \right\rangle, \qquad (1)$$

where $(\mathbf{R}_i, z_i) \equiv (x_i, y_i, z_i)$ are the molecular positions. The intrinsic profile does not depend on the sampled cross-sectional area $A_0$, and it should give a sharper view of the molecular structure at the interface. Within the CWT assumptions, the mean density profile,

$$\rho(z, A_0) = \left\langle \frac{1}{A_0} \sum_{i=1}^{N} \delta(z - z_i) \right\rangle, \qquad (2)$$

is the convolution of the intrinsic profile $\tilde{\rho}(z, q_u)$ with a Gaussian of square width given by the mean-square fluctuations of the intrinsic surface, $\Delta = \langle \xi^2 \rangle - \langle \xi \rangle^2$, that grows with the sample area as $\Delta(A_0, q_u) \approx \log[q_u \sqrt{A_0}/(2\pi)]/(2\pi\beta\gamma_0)$, in terms of the surface tension $\gamma_0$ and the usual inverse thermal energy $\beta = k_B T$.

For more than forty years, the presumably sharper view of the liquid surfaces given by $\tilde{\rho}(z, q_u)$ was not obtained from computer simulations, because of the lack of an explicit defi-

nition of the intrinsic surface $z = \xi(\mathbf{R}, q_u)$ to be associated to each molecular configuration. Different definitions give robust and sound results for the intrinsic surface Fourier components $\hat{\xi}_q$ at short wave vectors (for $q\sigma \ll 1$, in terms of the molecular diameter $\sigma$); but for $q\sigma \gtrsim 1$ the values of $\hat{\xi}_q$ depend strongly on the specific definition of the intrinsic surface.[4–6] This fact makes very difficult the theoretical link of the CWT with the density functional formalism,[7–9] and the development of intrinsic sampling methods for computer simulations.[3,10,11] The simplest definition of $\xi(\mathbf{R}, q_u)$, based on a local Gibbs dividing surface, fails to separate the bulk and surface fluctuations for $q\sigma \gtrsim 1$ and produce the spurious growth of short wavelength fluctuations. As a consequence,[5] the intrinsic density profiles Eq. (1) become increasingly smoother for larger $q_u$—i.e., instead of giving a sharper view of the molecular structure at the interface, they are more blurred than $\rho(z, A_0)$.

In order to solve that problem, it was necessary either to develop some approximate scheme[12] to separate the bulk and the surface contributions in the Gibbs dividing surface definition of $\xi(\mathbf{R}, q_u)$, or to search for alternative definitions pinned to the interface,[4–6] so that bulk fluctuations could be avoided from the beginning. In these later methods, the intrinsic surface is linked to a set of molecules chosen to represent the liquid surface, instead of relying on a density balance across the interface. This is done with a set operational rules to select the $N_s$ molecules taken to represent the "surface layer" in each sampled instantaneous configuration of the liquid interface. Once the molecules of the *surface layer* have been selected, the method has to provide additional rules to go from that discrete set of molecular positions $(\mathbf{R}_j, z_j)$, with $j = 1, .., N_s$, to the continuous representation of the intrinsic surface, $z = \xi(\mathbf{R}, q_u)$, to be used to get the intrinsic density profiles from Eq. (1) and to sample the statistical properties of the intrinsic surface.

Both the selection of the *surface layer* and the definition of the mathematical surface $z = \xi(\mathbf{R}, q_u)$, using the molecular positions of that layer as "surface pivots," are subject to some arbitrarily. Moreover, the specific set of rules used to

analyze the molecular configurations has to be applied with a reasonable computational cost, since we have to analyze several thousands of molecular configurations to get representative samplings. The first step uses some kind of percolation analysis to separate the main liquid cluster from isolated molecules, or small clusters, in the vapor; then the liquid molecules at the border of the main cluster are selected as representative of the surface. The first proposal in this sense was made in 1982 by Stillinger,[4] but only over the last few years there has been a broad search for efficient and computationally feasible methods for the intrinsic sampling of fluid interfaces. In a method devised for liquid-liquid interfaces[13,14] the analysis is restricted to the study of the intrinsic density profile, without any explicit choice for $\xi(\mathbf{R}, q_u)$, and a coarse version of the intrinsic profile is obtained for the molecules in one liquid referred to those in the other liquid. On the other hand, several approaches[15–17] focus on the identification of the layer but do not provide information on the intrinsic profiles. The intrinsic sampling method (ISM) was originally proposed by two of us[5,6] in an attempt to push the concepts of intrinsic surface and intrinsic density profiles to the sharpest possible level. This method is computationally more demanding than other recipes, but it is very versatile, working for free liquid surfaces as well as for liquid-liquid interfaces,[18–21] and it gives detailed information about surface layer particles as well as about the statistical properties of the intrinsic surface.

The main assumption of the ISM is that, with a careful definition of the intrinsic surface, the intrinsic density profile [Eq. (1)] may show a molecular layering structure. This structural feature of the liquid surfaces would be as generic as the oscillatory structure of the radial distribution function $g(r)$ is generic for bulk liquids, except very close to the critical temperature. The CW fluctuations erase that layering from the mean density profiles $\rho(z, A_0)$, unless the sampled area $A_0$ is very small or the surface very stiff. Within the present resolution of x-ray synchrotron beams, the surface layering is experimentally observable only in cold liquid metals,[22,23] or some exotic molecular liquids.[24] Computer simulations of some simple liquid models,[25,26] designed to have very low ratios between their triple and critical temperatures ($T_t/T_c \lesssim 0.15$), show the layering in $\rho(z, A_0)$ for a typical simulation box ($A_0 \sim 100\sigma^2$). However, for the Lennard-Jones (LJ) model of simple fluids the accessible temperatures for the liquid phase are much higher ($T_t/T_c \gtrsim 0.5$), the surface tension is lower, and the layering in $\rho(z, A_0)$ is fully damped by the CW for any $A_0 \gtrsim 10\sigma^2$, well below the acceptable size of the simulation boxes. The ISM allows to observe the intrinsic surface layering, independently of the box size, since the CW surface fluctuations are filtered out through Eq. (1).

The specific ISM recipes, used to select the molecules of the surface layer and the shape of the mathematical surface $z = \xi(\mathbf{R}, q_u)$ pinned to those "surface pivots," are based precisely on the search for the optimal deblurring of the intrinsic layering. In particular, a key element of the ISM analysis is the two dimensional density of the surface layer $n_s = N_s/A_0$, i.e., the number of molecules to be selected as belonging to the physical surface of the liquid, per unit of the nominal area $A_0$ of the interface. The optimal value of $n_s$ gives the

strongest intrinsic layering, and we claim that it represents a physical characteristic of the liquid surface, which depends on the molecular interactions and on the temperature. Such claim was supported by analysis of kinetic and dynamical properties of the surface, such as the diffusion of the molecules on the surface layer,[27] and the time autocorrelation function of the intrinsic surface Fourier components.[28]

In this work, we explore a different kinetic property of the surface, namely the rate at which the surface layer molecules, selected by the ISM in a molecular configuration, are replaced by other molecules in the successive time steps of the MD simulation. The minimum exchange rate provides a sharper definition for the optimal value $n_s$, and the comparison of the $n_s$ values obtained with different criteria gives a firmer basis to the method, which we have applied up to $T/T_c = 0.84$, when the weak surface layering gives not enough contrast to determine $n_s$ from the shape of the intrinsic density profiles.

In the next section, we give a brief review of the method, together with the details of the models and molecular dynamics (MD) simulations. The structural criterion for $n_s$ is reviewed in Sec. III, while in Sec. IV, we present the results for the molecular exchange rate at the surface. In Sec. V, we compare different parametric forms to define a mathematical surface $z = \xi(\mathbf{R}, q_u)$ from the discrete set of the surface layer molecules. Section VI gives the results of the hydrodynamic analysis of the surface fluctuations as an additional criterion to establish the physical value of $n_s$. The results obtained with the cross-check of the different criteria are discussed in Sec. VII, and we conclude with the perspectives opened by the method for the characterization of liquid surfaces.

## II. MODELS AND MOLECULAR DYNAMICS

We have studied the liquid-vapor interfaces of two different simple liquid models: the first one is the well known LJ potential (truncated at $r_c = 3.01\sigma$), with a ratio $T_t/T_c = 0.56$ between the triple and the critical temperatures. The stiffness of the LJ liquid surface, described by the surface tension in $kT/\sigma^2$ units, reaches its maximum value of $\gamma\sigma^2/(kT) = 1.36$ at its triple point temperature. The second model is the soft-alkali (SA) pairwise interaction potential,[25,26] with a soft repulsive core designed to give a low triple point temperature, with a ratio $T_t/T_c = 0.10$ similar to the experimental values of some liquid metals. The low-triple point temperature gives access to very stiff liquid surfaces, with $\gamma\sigma^2/(kT) = 10.7$, so that we may study liquid surfaces with very low-CW amplitudes.

In order to obtain dynamical information, canonical (NVT) MD simulations are performed, using the software package DL_POLY.[29] Our systems consist of a thick slab of liquid surrounded by vapor, with 2592 particles in a square box of dimensions $10.46\sigma \times 10.46\sigma \times 90\sigma$ for the LJ and $9.025\sigma \times 9.025\sigma \times 90\sigma$ for the SA. Periodic boundary conditions are employed in all three directions. The time step is set at a reduced value of $dt = 4.56 \times 10^{-3}\sigma\sqrt{m/\epsilon}$. We use a Nose-Hoover thermostat with a time constant $10dt$, and the systems are equilibrated for $10^6$ time steps.

A detailed account of the ISM procedure to obtain $\xi(\mathbf{R}, q_m)$ has been presented in Refs. 5, 6, and 18, the later

being the slight modification of the original procedure, which is used in the present work. The intrinsic surface for each sampled configuration of the liquid slab is described through its Fourier components:

$$\xi(\mathbf{R}, q_{\mathrm{u}}) = \sum_{|\mathbf{q}| \le q_{\mathrm{u}}} \hat{\xi}_q e^{i\mathbf{q}.\mathbf{R}}, \qquad (3)$$

with the sum over transverse wave vectors, $\mathbf{q} = 2\pi(n_x, n_y)/L_x$ and $n_x, n_y = 0, \pm 1, \pm 2 \ldots$, to include periodic boundary conditions on the transverse direction, in the computer simulation box. Note that these transverse wave vectors are specific to the simulation setup, and in particular the smallest wave vector in the CW spectrum is $2\pi/L_x$. On the other hand, there is some arbitrariness in the upper wave vector limit, $q_{\mathrm{u}}$, which determines the allowed level of corrugation of the intrinsic surface. In particular, the ISM requires to select a *maximum* level of resolution $q_{\mathrm{m}}$, or equivalently a cutoff wavelength $\lambda_{\mathrm{c}} = 2\pi/q_{\mathrm{m}}$ to define the sharpest allowed structure of the intrinsic surface. The classical choice within the CWT is to take the molecular size as cutoff wavelength, i.e., $\lambda_{\mathrm{c}} = \sigma$, since it would be meaningless to define a mathematical surface $z = \xi(\mathbf{R}, q_{\mathrm{u}})$ at a resolution level higher that the molecular reality behind it. We show here that within the ISM the natural choice for $\lambda_{\mathrm{c}}$ is indeed finely tuned to the molecular diameter.

At the maximum level of resolution the intrinsic surface $\xi(\mathbf{R}, q_{\mathrm{m}})$ is defined as that with the minimum area, within the restrictions to go exactly through all the selected surface layer particles ("pivots"), and to have null Fourier components for any wave vector $|\mathbf{q}| > q_{\mathrm{m}}$. The $N_{\mathrm{s}}$ surface pivots are selected in an iterative procedure, self-consistently with the shape of $\xi(\mathbf{R}, q_{\mathrm{m}})$ for each sampled configuration of the liquid slab. We first use a percolation analysis to eliminate any particle with less that three neighbors at distances below $1.5\sigma$. An initial set of surface pivots is selected as the most external molecules in each of the prisms arranged in a $4 \times 4$ mesh over the percolating liquid slab, and the initial intrinsic surface is the *minimal area* surface going through these $N_0 = 16$ initial pivot particles. Then we incorporate the particle, which is closest to the minimal surface as a new surface pivot, and recalculate the new intrinsic surface $\xi(\mathbf{R}, q_{\mathrm{m}})$, to go through all the previously selected pivots, plus the new one. This procedure is iterated until we reach a target occupation of the first layer $n_{\mathrm{s}} = N_{\mathrm{s}}/A_0$, which is the essential control parameter in the procedure.[18] Once the intrinsic surface for a given $n_{\mathrm{s}}$ is calculated, the contribution of that molecular configuration to the intrinsic density profile is evaluated using Eq. (1), where the average is made over 5000 configurations of the liquid slab, separated by 100 MD time steps. The intrinsic surface (3), and the intrinsic density profiles (1), for any wave vector cutoff $q_{\mathrm{u}} \le q_{\mathrm{m}}$ may be obtained with the restriction of the sum (3) to Fourier components with $q \le q_{\mathrm{u}}$.

We may get the intrinsic profile (1) and the statistical properties of the intrinsic surface (3) for any choice of the ISM parameters $n_{\mathrm{s}}$ and $\lambda_{\mathrm{c}} = 2\pi/q_{\mathrm{m}}$; now the problem is how to fix the optimum values of these control parameters. In this respect, we want to stress that the optimal $n_{\mathrm{s}}$ may be regarded as a physical property of the interface, the (projected)
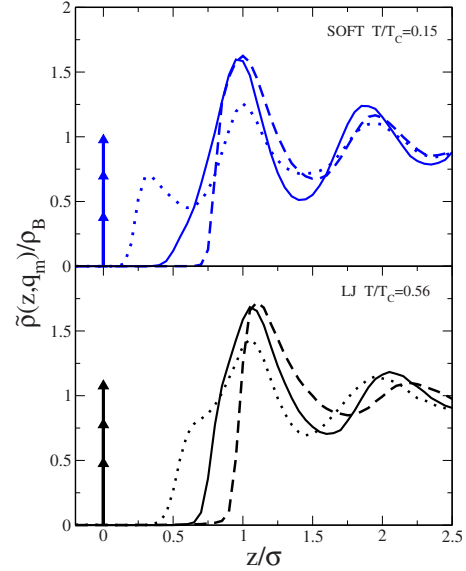


FIG. 1. (Color online) Intrinsic density profiles at the sharpest resolution $\tilde{\rho}(z, q_{\mathrm{m}})$, in density units relative to the bulk density. Top panel: results for the SA model at $T/T_{\mathrm{c}} = 0.15$, for three values of the two-dimensional density of the first layer $n_{\mathrm{s}}$. Dotted line: $n_0\sigma^2 = 0.4$, full line: $n_0\sigma^2 = 0.72$, and dashed line: $n_0\sigma^2 = 1.0$. Bottom panel: results for the LJ model at $T/T_{\mathrm{c}} = 0.56$. Dotted line: $n_0\sigma^2 = 0.5$, full line: $n_0\sigma^2 = 0.8$, and dashed line: $n_0\sigma^2 = 1.1$

density of molecules at the outmost layer of the liquid. On the other hand, $\lambda_{\mathrm{c}}$ is more an operational parameter of the ISM than a physical property of the surface. The only physical reality behind the mathematical surface $z = \xi(\mathbf{R}, q_{\mathrm{m}})$ is the discrete set of molecular positions through which it interpolates. The sharp truncation of the Fourier components at $q \le 2\pi/\lambda_{\mathrm{c}}$ and the requirement of minimal area within that constrain, are just reasonable choices for a smooth interpolation recipe. Therefore, we have run the whole ISM procedure for a set of $\lambda_{\mathrm{c}}$ values around the molecular diameter, and explore the dependence of the different properties, for the different temperatures and models, to discriminate its relevance.

## III. STRUCTURAL DETERMINATION OF $n_{\mathrm{s}}$

In the original ISM procedure,[5,18] $n_{\mathrm{s}}$ is fixed to get the highest possible contrast for molecular layers in the intrinsic profiles, without peculiar shoulders or any other unphysical feature. The results reported in this section correspond to the choice $\lambda_{\mathrm{c}} = \sigma$ for the wavelength cutoff, but they are nearly identical within a broad interval $0.6\sigma \lesssim \lambda_{\mathrm{c}} \lesssim 1.3\sigma$.

In Fig. 1, we present the intrinsic profiles at the maximum level of resolution $\xi(\mathbf{R}, q_{\mathrm{m}})$ for three different values of $n_{\mathrm{s}}$, both for LJ at $T/T_{\mathrm{c}} = 0.56$ and for SA at $T/T_{\mathrm{c}} = 0.15$, i.e., near their respective triple points. At this level of resolution the intrinsic surface goes precisely through the atoms of the outer liquid layer, so that the intrinsic profile has a delta-function peak, $n_{\mathrm{s}}\delta(z)$, corresponding to this surface layer, followed by a strongly oscillatory structure which decays toward the liquid bulk. The layering structure is weaker for the higher temperature of the LJ liquid ($T/T_{\mathrm{c}} \lesssim 0.56$), but
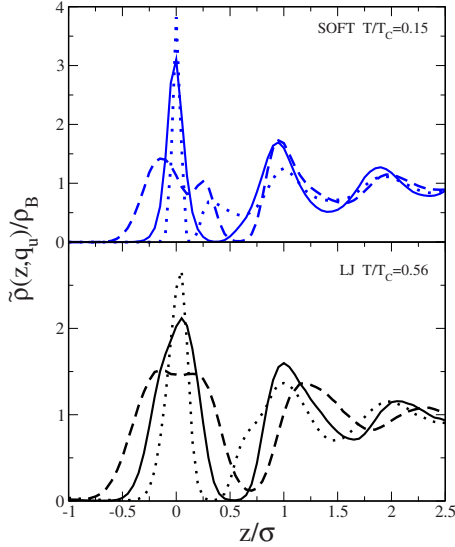
FIG. 2. (Color online). Intrinsic density profiles $\widetilde{\rho}(z,q_u)$ with $q_u = 2\pi/1.5\sigma$ relative to the bulk density. The notation is the same as in Fig. 1

still clearly visible and qualitatively similar to that of the cold SA liquid. On both systems, nonphysically low values of $n_s$ are signaled by the presence of a shoulder in the second layer of $\widetilde{\rho}(z,q_m)$, formed by molecules which should have been naturally assigned to the first, rather than to the second layer.

Unphysical large values of $n_s$ may be identified by the loss of the Gaussian shape of the second peak in $\widetilde{\rho}(z,q_m)$, with a very sharp slope, and by the damping of the oscillatory structure toward the liquid bulk. However, a better approach is to analyze the intrinsic profiles corresponding to intrinsic surfaces with a level of resolution lower that the maximum. These smoother intrinsic profiles, associated to any $q_u$ below $q_m$, are obtained with the same Fourier components as in $\xi(\mathbf{R},q_m)$ for $q < q_u$, but neglecting all those for $q \geq q_u$. Such surface $\xi(\mathbf{R},q_u)$ follows the longer wavelength fluctuations of the liquid surface, but does not go exactly through the atoms on the first layer, so that the delta-function first peak in $\widetilde{\rho}(z,q_m)$ becomes a broad peak, with increasing width as $q_u$ decreases. In Fig. 2, we compare $\widetilde{\rho}(z,q_u)$, with $q_u = 2\pi/1.5\sigma$ and three different values of $n_s$. For unphysical large values of $n_s$ the first peak of both liquids loses the Gaussian shape and splits into two secondary peaks, which indicates that some atoms assigned to this first layer must be assigned to the second layer. Therefore, by analyzing the intrinsic density profiles at different levels of resolution we can fix the occupation of the outer liquid layer. The optimum values of the surface density for the two system analyzed in this section are given in the first column of Table I. The procedure is quite robust for simple liquids up to $T/T_c \lesssim 0.7$, and it has been extended to realistic models of alkali metals,[20] water,[19] and to the dodecane-water interface.[21]

## IV. KINETIC DETERMINATION OF $n_s$

The determination of the parameter $n_s$ through the structure of the intrinsic profiles is very conclusive for the stiff

TABLE I. The surface layer density, $n_s\sigma^2$, in molecular diameter units, for LJ and SA models at several temperatures. The columns give the values with different criteria. From the structural properties we use the layering of the intrinsic profiles $\widetilde{\rho}(z,q_u)$. From the dynamical properties we use the minimum exchange rates $\Gamma(n_s,\sigma)$, with wavelength cutoff $\lambda_c = \sigma$, and with the majority rule $\langle\Gamma\rangle_{\lambda_c}$ (in brackets the percentage of common pivots for all the $\lambda_c$ values). Finally, in the last column, $n_s$ obtained from the equivalence between the structural and the hydrodynamic surface tensions, $\gamma_s(q) = \gamma_d(q)$.

| | Structural | Dynamic | | |
|---|---|---|---|---|
| $T/T_c$ | $\widetilde{\rho}(z,q_u)$ | $\Gamma(n_s,\sigma)$ | $\langle\Gamma\rangle_\lambda$ | $\gamma_d(q)$ |
| | | LJ model | | |
| 0.56 | $0.80 \pm 0.05$ | $0.77 \pm 0.03$ | 0.77 (93%) | |
| 0.63 | $0.75 \pm 0.05$ | $0.72 \pm 0.04$ | | 0.73 |
| 0.70 | $0.70 \pm 0.07$ | $0.66 \pm 0.05$ | | 0.67 |
| 0.77 | $0.65 \pm 0.10$ | $0.62 \pm 0.07$ | 0.60 (88%) | 0.62 |
| 0.84 | $0.60 \pm 0.15$ | $0.50 \pm 0.1$ | | |
| | | SA model | | |
| 0.15 | $0.72 \pm 0.025$ | $0.72 \pm 0.02$ | 0.72 (98%) | 0.74 |
| 0.21 | $0.72 \pm 0.03$ | $0.72 \pm 0.02$ | | |
| 0.27 | $0.72 \pm 0.04$ | $0.72 \pm 0.03$ | | |
| 0.33 | $0.72 \pm 0.05$ | $0.71 \pm 0.03$ | | |
| 0.39 | $0.70 \pm 0.05$ | $0.69 \pm 0.04$ | 0.73 (94%) | |
| 0.47 | $0.70 \pm 0.07$ | $0.70 \pm 0.05$ | | |
| 0.59 | $0.70 \pm 0.10$ | $0.65 \pm 0.07$ | | |
| 0.72 | $0.65 \pm 0.15$ | $0.60 \pm 0.10$ | 0.62 (91%) | |

surfaces of cold liquids, but the inherent disorder of the liquids precludes the precise determination of the optimal $n_s$ value beyond an error bar, which grows with the temperature. As shown in Table I, at $T/T_c \approx 0.7$ the relative incertitude is about 10% for the LJ model and even larger for the soft-core SA model. If $n_s$ is a physical parameter of the surface, and not a contrivance of the ISM procedure, its optimal value should be reflected in other features of the liquid surface. The aim of this section is to explore the kinetics of the surface layer molecules identified by the ISM, both to confirm the identification of the surface layer density as a physical property of the liquid interface and to explore alternative methods to get the optimal value of $n_s$.

Along molecular dynamics simulations we may study the dynamical properties of the surface particles (or "pivots"), which self-consistently define the intrinsic surface $\xi(\mathbf{R},n_s)$ in the ISM. In particular, after a time $\Delta t$ some of these molecules would have left the surface, either toward the inner liquid or toward the vapor, to be replaced by other molecules at the surface. The relative rate for this molecular exchange is given by $\Gamma(n_s,\lambda_c) = \Delta N_s/(N_s\Delta t)$, where $\Delta N_s$ is the mean number of surface layer molecules at time $t + \Delta t$ that were not associated to the surface layer at time $t$. The inverse $\Gamma^{-1}$ is the typical molecular exchange time at the surface. We make explicit the dependence of this surface exchange rate on the ISM parameters, $n_s$ and $\lambda_c$, since $\Gamma$ would obviously depend

on the operational procedure used to identify the surface layer molecules.

If we reduce the nominal value of $n_s$ below the real density of the outer liquid layer, then we expect that the ISM produces a rapid exchange in the list of $N_s = A_0 n_s$ surface pivots, since they would be a subset of the whole surface layer and very small changes on the shape of the intrinsic surface $z = \xi(\mathbf{R}, q_u)$ would change their selection. Therefore, we expect that $\Gamma(n_s, \lambda_c)$ grows when the nominal occupation is reduced below its physical value. On the other hand, if we set the occupation above its physical value, the ISM procedure would be forced to include in the list of "surface pivots" some molecules which belong to the inner layers, rather than to the outmost liquid layer. Again, the selection of the molecules in that list would be controlled by small changes in the shape of the intrinsic surface, and $\Gamma$ should grow with $n_s$. Therefore, we may expect that the optimum determination of the surface layer density $n_s$ gives the minimum surface exchange rate. Nevertheless, if $n_s$ is pushed too far above the density of a molecular monolayer, the nominal "surface layer" would become a thick liquid slab, and then we should expect that $\Gamma$ decreases like $1/n_s$, since the total exchange of molecules between that slab and the rest of the system, $\Delta N_s / \Delta t$ should depend on the area $A_o$, but not in the volume of the slab.

At each temperature, we have fixed the time interval between configurations $\Delta t$ in order that the average number of input/output pivots is less than 0.5, i.e., in more than half of the cases two successive configurations have the same $N_s$ molecules at the surface layer. This is important because if we use larger time intervals between configurations, the apparent value of $\Gamma$ decreases since between $t$ and $t + \Delta t$ some pivots exit and enter back in the pivot list, so that their contribution to $\Gamma$ is not detected. In terms of the MD time step $dt$, the typical time intervals between analyzed configurations are as follows: $\Delta t = 10 dt$ at low temperatures, $T/T_c = 0.15$; $\Delta t = 1 dt$ at $T/T_c = 0.47$; and $\Delta t = 0.1 dt$ at $T/T_c = 0.84$. For large $\Delta t$ we have analyzed the flux of pivots using the configurations separated a time interval $\Delta t$ obtained directly from MD simulations. However, for small $\Delta t$, and in order to improve averages over capillary wave fluctuations, we have carried out long MD simulations and kept every 100 or 1000 MD steps the position, velocity, and acceleration of all particles. For each one of these configurations we have calculated the new configuration for a time interval $\Delta t$ using the dynamical equations, and we have then calculated the flux of pivot between both configurations. Obviously, both procedures give the same results, but a good statistical average over CW fluctuations is computationally very expensive with the first method for low $\Delta t$.

Figure 3 presents the surface exchange rate for the cold SA liquid at $T/T_c = 0.15$ (top), and the LJ liquid at $T/T_c = 0.77$, well above its triple point temperature (bottom), for several wavelength cutoff $\lambda_c$. For nominal values of $n_s$ below the optimal structural range, and $\lambda_c \lesssim 1.2\sigma$, the surface exchange rate depends very little on $\lambda_c$. Larger values of $\lambda_c$ imply the use of fewer Fourier components in the description of the intrinsic surface (3) so that the restriction $z_i = \xi(\mathbf{R_i}, q_m)$, for all the $i = 1, \ldots, N_s$ surface pivots forces the surface $z = \xi(\mathbf{R}, q_m)$ to form blob shapes between the pivots,
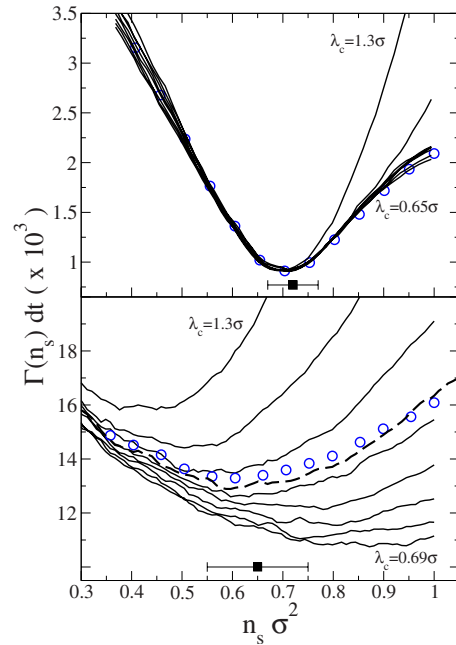


FIG. 3. (Color online) Pivot exchange frequency $\Gamma(n_s, \lambda_c)$, in units of the MD time step $dt$, as a function of the nominal surface layer density $n_s$. Full lines: results obtained for eight values of the *minimum* wavelength of corrugation $\lambda_c$ allowed to the intrinsic surface $\xi(\mathbf{R}, q_m)$ ($\lambda_c = \frac{L_x}{m}$ with the integer $m$ varying between $6 \leq m \leq 13$ for the SA model and between $7 \leq m \leq 14$ for the LJ). Circles: results using as pivots those which are pivots for most values of $\lambda_c$. Dashed lines: values obtained with $\lambda_c = \sigma$. The top panel shows results for the soft-alkali model at $T/T_c = 0.15$ and the bottom panel for the LJ model at $T/T_c = 0.77$. The full square and its error bar indicate the optimum surface layer occupancy determined by the structural procedure of Sec. III.

rather than being a smooth interpolation. Within the ISM, this over fitting of the intrinsic surface produces some randomness in the incorporation of new pivots for larger values of $n_s$, i.e., the method looses accuracy in the selection of the molecules of the surface layer, and the molecular exchange rate increases. On the contrary, low values of $\lambda_c$ imply that the parametric form (3) has many free variables $\hat{\xi}_q$ to get through all the pivots, and the additional requirement to have minimal area is very effective selecting the smoother possible shape. In this case, the small contributions from the large $q$ Fourier components make irrelevant to use a still larger number of Fourier components (i.e., a still lower $\lambda_c$ value), and the curves $\Gamma(n_s, \lambda_c)$ become roughly independent of the wavelength cutoff. The common trend of these curves is that, in agreement with our expectations, $\Gamma$ decreases as $n_s$ increases toward its optimal structural value.

For the stiff and strongly structured surface of the cold SA liquid we find that $\Gamma(n_s, \lambda_c)$ is nearly independent of the wavelength cutoff for $\lambda_c \lesssim 1.2$, even at very large nominal values of $n_s$. The common shape of these $\Gamma(n_s, \lambda_c)$ curves includes a clear minimum with respect to $n_s$, at a value within the optimal range selected in the previous section. The presence of such clear minimum in the surface molecular exchange is a strong confirmation that the concept of "surface layer" used by the ISM is a true physical reality, and it

offers an operational way to define the optimal density of that layer without the possible ambiguities in the selection of the optimal deblurring done in the structural characterization of $n_s$. Notice that for $n_s \gtrsim 0.9/\sigma^2$ the shape of $\Gamma(n_s, \lambda_c)$ becomes flatter, and further increase of the nominal occupation would eventually produce the expected change of the form into the $\sim 1/n_s$ decrease for a thick liquid slab.

For hotter and less structured surfaces, such as the SA model at higher temperatures and the LJ (bottom panel of Fig. 3), the shape of the function $\Gamma(n_s, \lambda_c)$ is more complex to analyze. The results for $n_s \lesssim 0.6/\sigma^2$ are roughly similar for any $\lambda_c \lesssim 1.2\sigma$, but for higher nominal occupations the surface exchange rate depends strongly on the wavelength cutoff. For any fixed $\lambda_c \gtrsim 0.65\sigma$ we still find a minimum exchange rate, but its position and value depend strongly on the wavelength cutoff. The interpretation for this dependence is that the higher molecular disorder in the hot liquid interface reduces the signal of the surface layering on $\Gamma(n_s, \lambda_c)$. There is a relatively large number of "interstitial" molecules, which may be considered either as part of the first or the second molecular layer, and their selection as surface pivots depends on the detailed shape of $\xi(\mathbf{R}, q_m)$, controlled by $\lambda_c = 2\pi/q_m$. Increasing $n_s$ with a low-wavelength cutoff produces the smooth incorporation of the interstitial molecules to the nominal surface layer, and it reduces the effect of the layering on $\Gamma(n_s, \lambda_c)$ for large $n_s$. On the contrary, large values of $\lambda_c$ produce rougher intrinsic surfaces, and the selection of surface pivots in the ISM becomes increasingly random for large $n_s$, as reflected by the growth of the exchange rate. The minimum of $\Gamma(n_s, \lambda_c)$ is at the optimal $n_s$, obtained from the shape of the intrinsic profiles, only when we set the wavelength cutoff very close to the molecular diameter, $\lambda_c = \sigma$.

The application of the ISM for hot liquid surfaces the structural determination of $n_s$ has a large uncertainty, hence it would be very useful to use the minimum of $\Gamma(n_s, \sigma)$ as a precise determination of the *optimal* $n_s$ value. However, that could only be achieved after accepting the fine tuning of $\lambda_c$ to the molecular diameter, since a 10% change (upwards or downwards) in the value of $\lambda_c$ produces important shifts in the value of $n_s$ at the minimum exchange rate. To that effect, we need a better discrimination on the "interstitial" molecules, which may be assigned to the first or to the second molecular layer depending on the detailed procedure used to interpret the surface layering structure. We may use the stability of the pivot list with respect to changes in the ISM parameter $\lambda_c$ to get a more robust determination of the surface layer molecules. We have used eight different values of $\lambda_c$, between $0.65\sigma$ and $1.3\sigma$, and for each sampled configuration and each nominal choice of $n_s$. Then considered that the $N_s = A_0 n_s$ "true" pivots are those selected by the majority of $\lambda_c$ values. That list includes a large proportion of pivots ($\approx 90\%$, as presented in Table I), which are common to all the fixed $\lambda_c$ lists. The strong dependence of $\Gamma(n_s, \lambda_c)$ on $\lambda_c$, observed for hot liquid surfaces at large $n_s$, is produced by a small proportion ($\sim 10\%$) of the selected surface layer molecules, which leave and re-enter the pivot list very rapidly. The list of the molecules in the majority of the fixed $\lambda_c$ lists is very robust with respect to the range of $\lambda_c$ values around $\sigma$. The surface exchange rate $\langle \Gamma(n_s) \rangle_{\lambda_c} = \Delta N_s/(N_s \Delta t)$, given by the time evolution of this majority pivot list is now free of
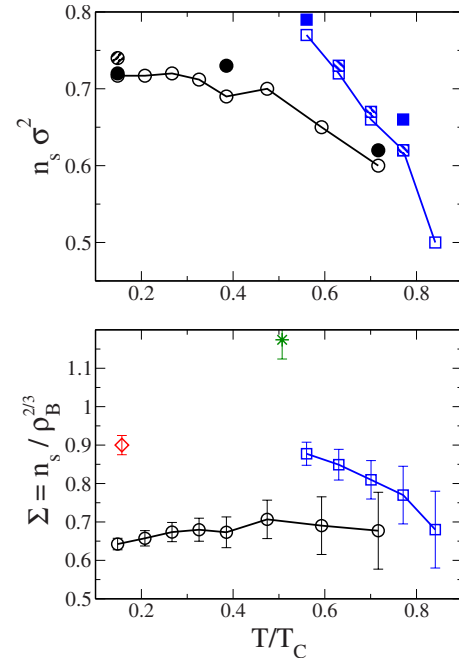


FIG. 4. (Color online) Top Panel: Two-dimensional density of the outer layer $n_s$ versus the temperature reduced by the critical one. Empty symbols: results with the kinetic criterion with $\lambda_{c0}$, full symbols: results obtained from $\langle \Gamma(n_s) \rangle_{\lambda_c}$, and semi-full symbols: hydrodynamic determination. Bottom Panel: the surface compactness $\Sigma \equiv n_s/\rho_B^{2/3}$ obtained using the kinetic criterion. Circles: SA model potential, squares: Lennard-Jones potential, star: SPC/E model of water, and rhombus: *ab initio* potassium. For the sake of clarity we have omitted the error bars at the top panel (see Table I).

the $\lambda_c$ parameter and it gives a cleaner view of its dependence with the nominal occupation $n_s$.

The circles of Fig. 3 show $\langle \Gamma(n_s) \rangle_{\lambda_c}$. For the strongly structured surface of the cold SA liquid (upper panels) the results are in full agreement with those of $\Gamma(n_s, \lambda_c)$ with any reasonable wavelength cutoff. For the hot LJ liquid surfaces (lower panels) $\langle \Gamma(n_s) \rangle_{\lambda_c}$ shows a clear minimum, which gives a very robust criterion to determine the optimum surface layer occupancy $n_s$, despite the inherent disorder and the weak layering structure of the intrinsic profile. The positions of that minimum, presented in Table I and shown in the top panel of Fig. 4, are within the wide range determined by the structural procedure explained in the previous section, and very close to those of $\Gamma(n_s, \sigma)$. Therefore, we may conclude that the optimal wavelength cutoff $\lambda_c$ is given by the molecular diameter $\sigma$ within an accuracy better than 10%, and that the optimal surface layer density $n_s$ may be obtained from the minimum exchange rate at the surface layer either with $\langle \Gamma(n_s) \rangle_{\lambda_c}$, or directly with $\Gamma(n_s, \sigma)$. The error bar for $n_s$ with this kinetic criterion may be systematically reduced increasing the number of configurations sampled with the ISM. Only for very high temperature, $T/T_c \gtrsim 0.85$, the position of the minimum of $\langle \Gamma(n_s) \rangle_{\lambda_c}$, starts to depend on the range of $\lambda_c$ used, and we cannot report an accurate value of $n_s$. This appears to be the limit for the application of the ISM. As explained above, the basic assumption of the method is that, with an appropriate filter for the CW fluctuations, the intrin-

sic density profiles in a liquid surface show the molecular layering structure. That assumption should fail as we approach the critical temperature, when the weaker intrinsic layering at the surface is overwhelmed by the inherent disorder of the liquid.

## V. COMPARISON WITH THE VORONOI SURFACE

The intrinsic density profiles and the surface layer exchange rate are properties directly related to the molecular positions, although selected and referred to the instantaneous position of the intrinsic surface $z = \xi(\mathbf{R}, q_{\mathrm{m}})$. In this and the following sections, we shift to the analysis of the statistical properties of that mathematical surface.

The ISM definition of $z = \xi(\mathbf{R}, q_{\mathrm{m}})$, as the minimal area surface connecting the *surface pivots* within a truncated Fourier series (3), is a reasonable criterion, but it is useful to have an independent assay comparing the intrinsic surface shape with other possible definition. Accepting that the selection of the *surface layer* molecules has been done, an (arguably) natural surface defined by a set of points is a three-dimensional triangulation (i.e., a triangulated surface, or mesh). This is a classic geometrical problem: given $N$ points, obtain the "best" triangulated surface that passes through them. There are many possible triangulation for a set of points, but there is (in practice) only one Delaunay triangulation, which is the "best" triangulation according to several criteria.[30] For example, for all triangular linear interpolations the Delaunay triangulation is the one with minimal roughness of the corresponding piecewise interpolant.[30] This triangulation is the dual of the three-dimensional Voronoi cell tessellation. To be more precise, we build a three-dimensional terrain from the two-dimensional Delaunay triangulation formed by projections of the pivots onto the $(x, y)$ plane.

Now we may ask how similar are the Delaunay triangulation and the intrinsic surface obtained using the Fourier parametrization (3). Thus, we have used the ISM to get the surface layer molecules and the intrinsic surface for a large sampling of configurations, over a mesh of values for $\lambda_{\mathrm{c}}$ and $n_{\mathrm{s}}$. For each configuration we have obtained the Delaunay triangulation and calculated the mean square distance between the two surfaces, interpolating over the same set of surface pivots. The lines $\lambda_{\mathrm{c}} = \lambda_{\mathrm{T}}(n_{\mathrm{s}})$ in Fig. 5 represent the wavelength cutoff giving the minimum distance between the ISM surface and the triangulation for each value of $n_{\mathrm{s}}$. As expected, a larger pivot density requires a shorter wavelength limit, i.e., more Fourier components in the series (3), to get similar descriptions with these rather different interpolation schemes between the $N_{\mathrm{s}} = A_o n_{\mathrm{s}}$ surface pivots. The relevance of this results comes from the fact that, for different models and temperatures, the lines $\lambda_{\mathrm{c}} = \lambda_{\mathrm{T}}(n_{\mathrm{s}})$ go always close to the point $(n_{\mathrm{s}}, \lambda_{\mathrm{c}} = \sigma)$ where $\Gamma(n_{\mathrm{s}}, \sigma)$ is minimum. This is also reflected in the values of $n_{\mathrm{s}}$ obtained from $\lambda_{\mathrm{T}}(n_{\mathrm{s}}) = \sigma$, which are always close to the structural and kinetic determinations of the surface layer density. Therefore, a comparison of the ISM $\xi(\mathbf{R}, q_{\mathrm{m}})$ with the three-dimensional triangulation confirms again the choice of the parameter $\lambda_{\mathrm{c}}$ close to the molecular size, and it gives support to the ISM smooth interpolation between the molecules of the surface layer.
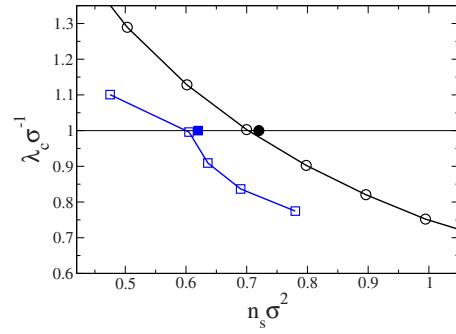


FIG. 5. (Color online) The empty symbols show the *minimum* wavelength of corrugation $\lambda_{\mathrm{T}}$ allowed to our Fourier parameterization of the intrinsic surface of $\xi(\mathbf{R}, q_{\mathrm{m}})$ in order to obtain the best fits of that to a Delaunay triangulated surface, as a function of the two-dimensional density of the outer layer $n_{\mathrm{s}}$. Circles: results for the SA model at $T/T_{\mathrm{c}} = 0.15$, and squares: LJ model at $T/T_{\mathrm{c}} = 0.77$. The full symbols are the optimal values of $n_{\mathrm{s}}$ obtained with the study of the kinetics of pivots using as wavelength cutoff $\lambda_{\mathrm{c}} = \sigma$.

## VI. HYDRODYNAMIC ANALYSIS

The statistical properties of the intrinsic surface may be directly sampled along MD simulations using any operational definition for $\xi(\mathbf{R}, q_{\mathrm{u}})$. The classical CWT predicts independent Gaussian probabilities for the Fourier components $\hat{\xi}_q$, with mean square modulus $\langle |\hat{\xi}_q|^2 \rangle = k_{\mathrm{B}} T / (\gamma_0 A_0 q^2)$, in terms of the (macroscopic) surface tension, $\gamma_0$. The results for $\langle |\hat{\xi}_q|^2 \rangle$ obtained from computer simulations, and from the interpretation of x-ray surface diffraction data, deviate from that prediction for $q\sigma \gtrsim 1$, and they are usually described by an effective wave vector dependent *structural* surface tension,[6,18]

$$\gamma_{\mathrm{s}}(q) \equiv \frac{k_{\mathrm{B}} T}{q^2 \langle |\hat{\xi}_q|^2 \rangle A_0}. \tag{4}$$

However, different operational definitions of the intrinsic surface give qualitatively different shapes for $\gamma_{\mathrm{s}}(q)$, except at the $q = 0$ limit set by the macroscopic surface tension. That has created a controversy, with claims[8,31] and refusals[9,32] for an enhanced CW regime at nanometric scale, characterized by a local minimum of $\gamma_{\mathrm{s}}(q)$. Even within the restricted range of the ISM definitions for $\xi(\mathbf{R}, q_{\mathrm{u}})$, the values of $\gamma_{\mathrm{s}}(q)$ from Eq. (4) show a strong dependence on the choice for the parameters $n_{\mathrm{s}}$ and $\lambda_{\mathrm{c}}$, so that the "physical" dependence of the surface tension with $q$ could only be obtained (or assumed) after a physical choice for these parameters of the method.

The analysis of a different statistical property of the intrinsic surface may lead to a complementary, and more robust, determination of $\gamma(q)$.[28] Along the MD simulation we may keep track of the time dependence of the intrinsic surface Fourier components, $\hat{\xi}_q(t)$, to obtain their autocorrelation function $\langle \hat{\xi}_q(t+t') \hat{\xi}_q^*(t') \rangle - \langle |\hat{\xi}_q(t)|^2 \rangle$. In the macroscopic hydrodynamic regime this autocorrelation function may be obtained from the surface tension, mass density and viscosity of the liquid; the deviation from that prediction in the MD results for $q\sigma \gtrsim 1$ may be interpreted as in terms of a *dy-*
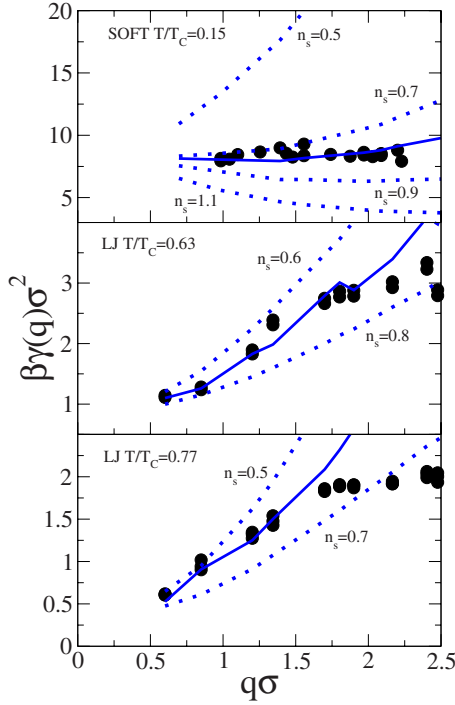
FIG. 6. (Color online) Effective wave-vector-dependent surface tension $\gamma(q)$. The circles show the hydrodynamical $\gamma_d(q)$, obtained by numerical inversion of the hydrodynamic relation for the decay of the surfaces modes (Ref. 28), for several choices of the parameter $n_s$ around its optimal value. The full lines correspond to the equilibrium $\gamma_s(q)$ at the optimal occupation $n_s$, for which $\gamma_s(q)$ agrees better with the hydrodynamical $\gamma_d(q)$. The values of the hydrodynamical optimal occupations are given in the last column of Table I. Top panel: SA model at $T/T_c=0.15$, middle panel, LJ model at $T/T_c=0.63$, and bottom panel, LJ model at $T/T_c=0.77$. The dotted lines show the equilibrium $\gamma_s(q)$ for $n_s$ away from its optimal value.

*namic* wave vector dependent surface tension $\gamma_d(q)$. Figure 6 shows how $\gamma_d(q)$ depends very little on the choice of the ISM parameter $n_s$, and that it agrees with the *structural* $\gamma_s(q)$ only when $n_s$ is fixed at (or very near) its optimal value. This agreement is observed for $q \lesssim 1.7$, at larger $q$ the decorrelation of surfaces modes gradually becomes controlled by molecular diffussion rather than by surface tension hydrodynamics.[28] Such agreement, for different temperatures and model interactions, provides a strong support to the ISM as operational definition of the intrinsic surface, and to the values obtained for the surface layer density as presented in Table I and in the top panel of Fig. 4.

## VII. RESULTS AND DISCUSSION

In the previous sections, we have verified that within the ISM analysis of MD simulations for liquid surfaces, the surface layer density $n_s$ may be consistently obtained from very different properties: the layering of the intrinsic density profiles, the minimum exchange rate of the molecules at the surface layer, and the decay time of the autocorrelation function for the intrinsic surface Fourier components $\hat{\xi}_q(t)$. Also,

the similarity of the intrinsic surface $z=\xi(\mathbf{R}, q_u)$ and a Voronoi triangulation with the same set of surface pivots, gives support to the ISM recipes to select those pivots and to interpolate between them with a Fourier series truncated at wavelengths below the molecular diameter. Altogether, this extensive analysis provides a strong evidence that the method is extracting relevant *intrinsic* features of the liquid surfaces. The usual description in terms of mean density profiles, blurred by the CW fluctuations Eq. (2), implies a severe lost of this information.

In this section, we proceed to discuss the model and temperature dependence of the liquid surfaces in terms of their three main intrinsic properties: How many molecules lie at the interface, as given by the surface layer density $n_s$; what is the mean instantaneous area of the surface $\langle A_\xi \rangle$, relative to the macroscopic (cross sectional) area $A_o$; and what is the typical exchange rate of these molecules at the surface, as given by the minimum values of $\Gamma(n_s, \sigma)$.

### A. Surface layer density and compactness

The upper panel in Fig. 4 presents $n_s \sigma^2$, as function of $T/T_c$, for the LJ and SA models. We use the values obtained from the kinetic analysis, to get shorter error bars, but the results from the other methods are very similar, as shown in Table I. The two models give surface layer densities that decrease with increasing temperature, although this trend is clearly stronger for LJ than for SA. The lower panel presents the results for $n_s$ scaled with the liquid bulk density $\rho_B$, to get a dimensionless index for the surface compactness $\Sigma \equiv n_s / \rho_B^{2/3}$.

The SA model, with ultrasoft core interactions, has $\Sigma \approx 0.67 \pm 0.03$ nearly constant over the whole temperature range $0.15 \leq T/T_c \leq 0.72$. The LJ surface converges toward similar values at high temperature, but it goes up to $\Sigma \approx 0.87$ at the triple point. The two isolated points in the bottom panel of Fig. 4 correspond to the ISM results for other liquid surfaces which had been previously reported[19,20] and reanalyzed here: the SPC/E model for water at $T=330$ K$=0.51T_c$ gives $n_s \sigma^2=1.15 \pm 0.05$ and $\Sigma \approx 1.17$, while the liquid metal surface of an *ab initio* model of potassium has $n_s \sigma^2=0.9 \pm 0.03$ and $\Sigma \approx 0.9$ at $T=343$ K$=0.16T_c$ near its triple point.

A geometrical interpretation for $\Sigma$ is obtained from crystal surfaces. The most compact surfaces of close packed lattices, like the {111} face in the FCC structure, have $\Sigma=0.9165$, while for the BCC lattice the highest value ($\Sigma=0.890$) is given by the {110} face. These values are similar to those observed in the LJ and liquid potassium surfaces near their triple points. At higher temperature, the LJ surface compactness decays toward values similar to the SA model, close to the open {100} face of the BCC lattice, $\Sigma=0.630$. In contrast, the dense surface of water has $\Sigma \approx 1.17$, clearly above any FCC or BCC crystal face, although below the compact {100} face of the open diamond structure ($\Sigma=1.33$). Of course, we cannot expect a full correspondence between the correlated disorder in a liquid surface and the geometrical arrangements of crystal lattices, but still the values of $\Sigma \equiv n_s / \rho_B^{2/3}$ provide a quantitative view of how the neighbor shell in the liquid bulk

is broken at the surface, exposing compact or sparser "faces" for different molecular interactions and temperatures.

In particular, the high-surface compactness of water correlates well with other peculiarities. The structure of the intrinsic profiles,[19] shows a dense and very well-defined first liquid layer, followed by a very rapid damping of the oscillatory structure beyond the first layer, due to the open correlation structure created by directional bonding; and these intrinsic profiles are very similar in the free (liquid-vapor) surface and that at oil-water interfaces.[21] Also, the minimum of the surface exchange rate $\Gamma(n_s, \sigma)$ in water is less pronounced than the minimum of $\Delta N_s = n_s \Gamma(n_s, \sigma) A_o \Delta t$, contrary what is observed in the other models.

At high temperature, the apparent convergence of the LJ and SA results could be extrapolated to a critical surface compactness in the range $0.6 \lesssim \Sigma \lesssim 0.7$, which may be the geometrical result of a loose arrangement of the nearest neighbors. The ultra-soft repulsion of the SA model would produce that $\Sigma$, even at high density (low $T/T_c$), while the LJ approaches the same value only near $T_c$, when the low density has relaxed the packing constrains on the shell of neighbors. That assumption could open the extension of the ISM toward the critical region, with the definition of the intrinsic surface as the minimal area surface going through a prefixed number of surface pivots $N_s = n_s A_o \approx 0.65 \rho_B^{2/3} A_o$, so that we do not have to relay in the existence of a surface layering structure to find the optimal value of $n_s$.

### B. Surface roughness

A complementary view of the liquid surfaces is given by their roughness, defined as the relative increase of surface area with respect to the projected area,

$$\Delta_A = \frac{\langle A_\xi \rangle - A_0}{A_0}, \tag{5}$$

where the mean intrinsic surface area $\langle A_\xi \rangle$ is

$$\langle A_\xi \rangle = \left\langle \int d^2\mathbf{R} \sqrt{1 + |\nabla_\mathbf{R} \xi(\mathbf{R})|^2} \right\rangle \approx A_o + \frac{A_o}{2} \sum_{0 < |\mathbf{q}|}^{q_u} q^2 \langle |\hat{\xi}_q|^2 \rangle. \tag{6}$$

The top panel in Fig. 7 shows the values of $\Delta_A$ for the same models and temperatures presented in Fig. 6. For the stiff surfaces of the SA model or potassium, near their triple points, the mean area $\langle A_\xi \rangle$ is less than 10% above the projected value $A_0$. However at $T/T_c = 0.84$ the LJ surface has more than 30% increase over its nominal area. In the later case, the quadratic approximation in Eq. (6) may be questioned.

In terms of the structural surface tension (4) we have

$$\Delta_A \approx \frac{1}{2} \sum_{|\mathbf{q}| < q_u} q^2 \langle |\hat{\xi}_q|^2 \rangle = \frac{k_B T}{2 \gamma_0 A_0} \sum_{0 < |\mathbf{q}|}^{q_u} \frac{\gamma_0}{\gamma(q)}. \tag{7}$$

The classical form of the CWT assumes that $\gamma(q) = \gamma_0$ for any $|\mathbf{q}| < 2\pi/l_{cw}$, with an effective wavelength cutoff $l_{cw}$, which would lead to the same roughness as the full spectrum with $\gamma(q)$ extended up to $q = 2\pi/\lambda_c = 2\pi/\sigma$.
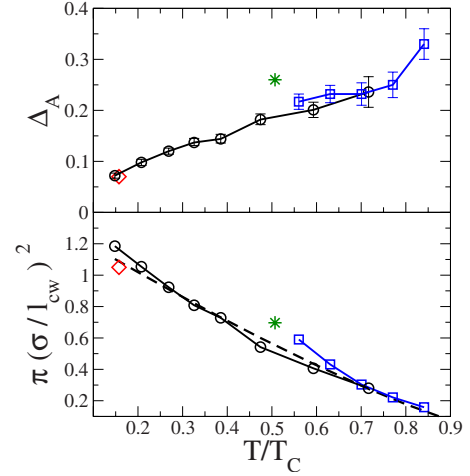


FIG. 7. (Color online) Top panel: Roughness, defined as $\Delta_A = \langle A_\xi \rangle / A_0 - 1$ versus temperature reduced by the critical one. Bottom panel: The effective number of CWT surface modes per $\sigma^2$ area, Eq. (8). Circles: SA model potential, squares: Lennard-Jones potential, star: SPC/E model of water, and rhombus: *ab initio* potassium. In the bottom panel the dashed line shows the fit $\propto (1 - \frac{T}{T_C})^{1.26}$ suggested by the scaling of $l_{cw}$ as the bulk correlation length.

The sum in the last term of Eq. (7) is just the effective number of CW modes which should be used to describe the intrinsic surface fluctuations in the classical version of the CWT. In the continuous limit we get

$$\frac{1}{A_0} \sum_{|\mathbf{q}| < 2\pi/\sigma} \frac{\gamma_0}{\gamma(q)} \equiv \frac{1}{A_0} \sum_{|\mathbf{q}| < 2\pi/l_{cw}} \approx \frac{\pi}{l_{cw}^2}, \tag{8}$$

effective surface modes per unit area. Then Eq. (7) may be interpreted as the classical equipartition result, with the mean (free) energy of the CW given by $\gamma_0(\langle A_\xi \rangle - A_0)$ and equal to $k_B T/2$ times the number of surface modes.

The lower panel in Fig. 7 shows that, for all the models and temperatures explored here, the effective number of classical CW modes per $\sigma^2$ area, i.e., $\pi(\sigma/l_{cw})^2 \equiv 2\Delta_A \gamma_0 \sigma^2/(k_B T)$, fall roughly into a common curve, decaying toward zero at $T/T_C$. Thus, in the approach to the critical point, the roughness of the interface $\Delta_A$ increases but the surface tension $\gamma_0(T)$ decreases faster. The quantitative analysis of the critical behavior for $\Delta_A(T)$ and $l_{cw}(T)$ is beyond the scope of this paper, but the decay of $\pi(\sigma/l_{cw})^2$ extracted here through the ISM analysis of the MD simulations, is in qualitative agreement with the proposals of mesoscopic theories for CW fluctuations near the critical point,[33,34] which assume that the effective CW cutoff $l_{cw}$ should be proportional to the bulk correlation length. That suggests the fit $\pi(\sigma/l_{cw})^2 \approx 1.35(1 - T/T_c)^{1.26}$ presented in the bottom panel of Fig. 7, and reasonably accurate over the full range of temperatures.

Notice that the ISM avoids any coarse graining. The nominal resolution of the intrinsic surface is kept at molecular scale at any temperature, since the shape of $z = \xi(\mathbf{R}, q_m)$ includes Fourier components with wavelength above $\lambda_c \equiv 2\pi/q_m = \sigma$. However, the results extracted from the ISM analysis of MD simulations show that for large wave vectors
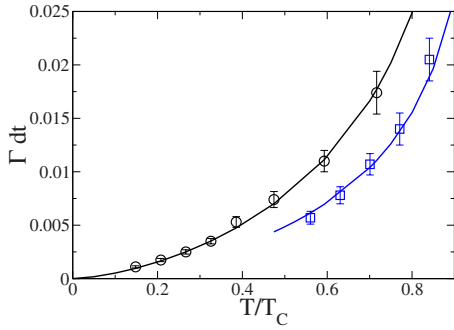
FIG. 8. (Color online) The surface molecules exchange rate $\Gamma$ in units of the MD time step d$t$, versus temperature reduced by the critical one. Circles: SA model potential, squares: Lennard-Jones potential. The lines show the $\Gamma dt \propto T^{1.5}(1-\frac{T}{T_C})^{-0.5}$ fits.

the intrinsic surface Fourier components decay much faster than the classical prediction $\langle |\hat{\xi}_q|^2 \rangle \sim 1/q^2$, as it is represented by the increase in $\gamma(q)$ obtained from Eq. (4). Therefore, the application of the method at increasing temperatures *extracts* in $\gamma(q)$ the two physical characteristics, which had to be *assumed* in the mesoscopic theories of CW fluctuations:[33,34] as $T \to T_c$, the surface becomes softer at large scales [$\gamma_0 = \gamma(0) \sim (T_c - T)^\mu$, with $\mu \approx 1.26$], but at the same time the surface becomes stiff [high $\gamma(q)$] at wavelengths below an increasingly large cutoff, defined by the effective CWT parameter $l_{cw}$ defined through Eq. (8).

The conjecture of a *geometrically fixed* critical value for $n_s/\rho_B^{2/3}$ made in the previous subsection could open the route for a quantitative check of the assumption $l_{cw} \sim (T_c - T)^{-\nu}$, with the bulk correlation length exponent $\nu \approx 0.63$. If that were the case, the combined critical exponent for $\Delta_A \sim 1/(\gamma_0 l_{cw}^2) \sim (T_c - T)^{2\nu - \mu}$, would vanish (in $d=3$ dimensions) by the hyperscaling relation $\mu = (d-1)\nu$, leaving a weak logarithmic divergence (or a finite limit) for the ISM surface roughness.

### C. Rate of molecular exchange at the surface

Finally, we consider the ISM results for the surface exchange rate $\Gamma$ as a function of $T/T_c$, for the SA and LJ models. This is a specific property of the kinetic analysis of liquid surfaces, closely related to the analysis of the surface diffusivity,[27] but very distinct from the structural properties described above.

Figure 8 presents the results for $\Gamma(n_s, \sigma)$d$t$, with the MD time step d$t = 4.56 \times 10^{-3} \sigma \sqrt{m/\epsilon}$. This dimensionless rate increases with $T/T_c$, from $10^{-3}$ for the SA surface at $T/T_c = 0.15$, to 0.02 for LJ at $T/T_c = 0.84$; with the results for LJ always below those of the SA model at the same relative temperature. Taking the mass and the LJ parameters to represent argon, the typical residence time of the atoms at the surface is $\tau = \Gamma^{-1} \approx 2$ picoseconds (ps) at $T/T_c = 0.56$, and 0.5 ps at $T/T_c = 0.84$; to be compared with 4 ps for SPC/E water model[19] at $T/T_c = 0.50$, and 8 ps for potassium at $T/T_c = 0.15$ in an *ab initio* model.[20]

The increase of the surface exchange rate with the temperature has a low $T$ regime with $\Gamma \sim T^{3/2}$, observed for the

SA model at $T/T_c \lesssim 0.4$, but inaccessible to the LJ liquid. The high temperature behavior is more puzzling, since the fits of the data of Fig. 8 shows the apparent divergence $\Gamma \sim (T_c - T)^{-\theta}$, with $\theta \approx 0.5 \pm 0.1$, for both models. The extension of the ISM to the critical temperature could eventually discern if the apparent growth of $\Gamma$ is a critical divergence or not. Here, we can only speculate with the possible interpretations of a result that is not yet confirmed.

The self-diffusion constant of the molecules at the critical point remains finite, although with diverging derivatives with respect to temperature and density. The dynamics of large correlation patterns should reflect the critical slowing down, with longer times for changes at larger scale. The ISM is a link between the molecular positions and the shape of an intrinsic surface, with an operational set of rules to perform a mesoscopic analysis of the interface. Therefore, it is not obvious why the exchange rate of the molecules selected as "surface pivots" may diverge at $T_c$. This question is particularly relevant since in this paper, we have shown that the optimal choice for the ISM parameter $n_s$ may be obtained very precisely at the minimum of $\Gamma(n_s, \sigma)$. That criterion was based on the existence of intrinsic surface layering, which we have been unable to apply for $T/T_c > 0.85$. The rapid increase of $\Gamma$ in Fig. 8 could be just a signal for the physical limits of the ISM assumptions, and that the method of analysis cannot be used closer to $T_c$, since the concept of "surface layer" loses its physical significance.

Alternatively, we may speculate that a critical surface compactness $\Sigma \approx 0.65$ could be used, within the ISM rules, without relying on the layering of intrinsic density profiles. Then, properties such as $\Delta_A$, $l_{cw}$, and $\Gamma$ could be explored in MD simulations near the critical point, within a controlled definition of the intrinsic surface. In that case, the critical divergence of $\Gamma$ could perhaps reflect the divergence of $l_{cw}$, i.e., the short scale "flatness" of the intrinsic surface defined through the ISM recipe. The increasingly large scale for that local rigidity, together with the soft fluctuations at large scale, may produce the divergence of the exchange rate for the molecules in the list of surface pivots.

### VIII. CONCLUSIONS

The first conclusion from this work is that, with the adequate deblurring of the CW effects, liquid surfaces show a molecular layering structure that may be used to define an intrinsic surface, at least up to $T/T_c \approx 0.85$. The study of the kinetics of the pivots (molecules that belong to the surface layer) shows that their exchange rate, as a function of the two-dimensional density of the outer liquid layer $n_s$, exhibits a clear minimum at the optimum value of $n_s$. This fact confirms that $n_s$ is an inherent physical property of the atomic structure of the liquid surface. The claim is supported by the good agreement, for all systems and temperatures studied, between the kinetic $n_s$ values and those obtained using other alternative procedures: the strongest layering in the intrinsic density profiles,[18] the largest diffusion times of molecules across the intrinsic surface,[27] and the best (almost perfect) agreement between the hydrodynamical and the structural predictions for the effective wave-vector dependent surface tension $\gamma(q)$.[28]

For the practical application of the ISM, the analysis of the surface exchange rate is the best way to determine $n_s$, and at the same time it gives a fine tuning of the wavelength cutoff at the molecular diameter $\lambda_c \equiv 2\pi/q_m = \sigma$, to complete the operational parameters of the method. Only at $T/T_c \lesssim 0.6$ the direct inspection of the intrinsic profiles may be equally precise and computationally cheaper.

After the accumulation of evidence for the inherent physical character of $n_s$, and its precise determination with the application of the ISM at high temperatures, we have explored the view of liquid surfaces which emanates from their intrinsic properties. The growth of the surface roughness with $T/T_c$ follows an approximate universality, with similar values for different models. However, the surface compactness reflects clearly the effects of the molecular interactions, and it gives a quantitative view of how the shell of neighbors in the bulk liquid is broken at the surface, exposing compact or sparse "faces." Together with the surface exchange rate, these intrinsic properties of the liquid interfaces may help us understand the physical and chemical processes taking place in these systems. Still many questions remain open, particularly in the approach to the critical region, and further work is required to explore the possible application of the intrinsic sampling method in those conditions.

*echacon@icmm.csic.es

†Present address: Dpto. Enseñanzas Básicas de la Ingeniería Naval, ETS Ingenieros Navales, Avd. Arco de la Victoria, s/n E-28040 Madrid Spain.

[1] F. P. Buff, R. A. Lovett, and F. H. Stinger, Phys. Rev. Lett. **15**, 621 (1965).

[2] R. Evans, Adv. Phys. **28**, 143 (1979).

[3] J. R. Percus, in *Fluid Interfacial Phenomena*, edited by C. A. Croxton (Wiley, New York, 1986), pp. 1–44.

[4] F. H. Stillinger, J. Chem. Phys. **76**, 1087 (1982); F. H. Stillinger and J. D. Weeks, *ibid.* **99**, 2807 (1995).

[5] P. Tarazona and E. Chacón, Phys. Rev. B **70**, 235407 (2004).

[6] E. Chacón and P. Tarazona, Phys. Rev. Lett. **91**, 166103 (2003).

[7] K. Katsov and J. D. Weeks, J. Phys. Chem. B **106**, 8429 (2002).

[8] K. R. Mecke and S. Dietrich, Phys. Rev. E **59**, 6766 (1999).

[9] P. Tarazona, R. Checa, and E. Chacón, Phys. Rev. Lett. **99**, 196101 (2007).

[10] J. Stecki, J. Chem. Phys. **109**, 5002 (1998).

[11] A. Werner, F. Schmid, M. Müller, and K. Binder, Phys. Rev. E **59**, 728 (1999).

[12] E. M. Blokhuis, J. Kuipers, and R. L. C. Vink, Phys. Rev. Lett. **101**, 086101 (2008); E. M. Blokhuis, J. Chem. Phys. **130**, 014706 (2009).

[13] J. Chowdhary and B. M. Ladanyi, J. Phys. Chem. B **110**, 15442 (2006).

[14] M. Jorge and M. N. D. S. Cordeiro, J. Phys. Chem. C **111**, 17612 (2007).

[15] L. B. Pártay, G. Hantal, P. Jedlovszky, A. Vincze, and G. Horvai, J. Comput. Chem. **29**, 945 (2008).

[16] D. I. Zhukhovitskii, J. Chem. Phys. **125**, 234701 (2006).

[17] J. Chowdhary and B. M. Ladanyi, Phys. Rev. E **77**, 031609 (2008).

[18] E. Chacón and P. Tarazona, J. Phys.: Condens. Matter **17**, S3493 (2005).

[19] E. Chacón, P. Tarazona, and J. Alejandre, J. Chem. Phys. **125**, 014709 (2006).

[20] E. Chacón, P. Tarazona, and L. E. Gonzalez, Phys. Rev. B **74**, 224201 (2006).

[21] F. Bresme, E. Chacón, P. Tarazona, and K. Tay, Phys. Rev. Lett. **101**, 056102 (2008); Phys. Chem. Chem. Phys. **10**, 4704 (2008).

[22] O. M. Magnussen, B. M. Ocko, M. J. Regan, K. Penanen, P. S. Pershan, and M. Deutsch, Phys. Rev. Lett. **74**, 4444 (1995); E. DiMasi, H. Tostmann, B. M. Ocko, P. S. Pershan, and M. Deutsch, Phys. Rev. B **58**, R13419 (1998).

[23] M. J. Regan, E. H. Kawamoto, S. Lee, P. S. Pershan, N. Maskil, M. Deutsch, O. M. Magnussen, B. M. Ocko, and L. E. Berman, Phys. Rev. Lett. **75**, 2498 (1995).

[24] H. Mo, G. Evmenenko, S. Kewalramani, K. Kim, S. N. Ehrlich, and P. Dutta, Phys. Rev. Lett. **96**, 096107 (2006); H. Mo, S. Kewalramani, G. Evmenenko, K. Kim, S. N. Ehrlich, and P. Dutta, Phys. Rev. B **76**, 024206 (2007).

[25] E. Chacón, M. Reinaldo-Falagán, E. Velasco, and P. Tarazona, Phys. Rev. Lett. **87**, 166101 (2001).

[26] E. Velasco, P. Tarazona, M. Reinaldo-Falagán, and E. Chacón, J. Chem. Phys. **117**, 10777 (2002).

[27] D. Duque, P. Tarazona, and E. Chacón, J. Chem. Phys. **128**, 134704 (2008).

[28] R. Delgado-Buscalioni, E. Chacón, and P. Tarazona, Phys. Rev. Lett. **101**, 106102 (2008); J. Phys.: Condens. Matter **20**, 494229 (2008).

[29] W. Smith, Mol. Simul. **32**, 933 (2006).

[30] CGAL User and Reference Manual, CGAL Editorial Board, 3.4, (2008), http://www.cgal.org/Manual/3.4/doc /html/cgal/manual/packages.html

[31] C. Fradin, A. Braslau, D. Luzet, D. Smilgies, M. Alba, N. Boudet, K. Mecke, and J. Daillant, Nature (London) **403**, 871 (2000).

[32] P. S. Pershan, Colloids Surf., A **171**, 149 (2000); O. Shpyrko, M. Fukuto, P. Pershan, B. Ocko, I. Kuzmenko, T. Gog, and M. Deutsch, Phys. Rev. B **69**, 245423 (2004).

[33] J. D. Weeks, J. Chem. Phys. **67**, 3106 (1977).

[34] J. V. Sengers and J. M. J. vanLeeuwen, Phys. Rev. A **39**, 6346 (1989).